

Computational Interpretation of Megagauss-Magnetic-Field-Induced Metallic Surface Plasma Initiation and Evolution

Irvin R. Lindemuth, Richard E. Siemon, Bruno S. Bauer, and Milena A. Angelova
University of Nevada, Reno, Nevada, USA

Walter L. Atchison

Los Alamos National Laboratory, Los Alamos, New Mexico, USA
(Received 22 April 2010; published 2 November 2010)

Numerical simulations of experiments in which plasma is formed on an aluminum surface by megagauss magnetic fields provide the first computational demonstration of a magnetic-field threshold that must be reached for aluminum plasma to begin to form. The computed times of plasma initiation agree reasonably well with the observations across the full range of rod diameters, leading to the conclusion that plasma formation is a thermal process. Computationally, plasma forms first in low-density material that is resistive enough to expand across the magnetic field and yet conductive enough that Ohmic heating exceeds expansion cooling.

DOI: [10.1103/PhysRevLett.105.195004](https://doi.org/10.1103/PhysRevLett.105.195004)

PACS numbers: 52.25.-b, 52.50.-b, 52.58.Lq, 52.65.Kj

Understanding the physical processes that can lead to the formation of plasma on the surface of metals subjected to megagauss magnetic fields and magnetic pressures of 100 kbar and more, and understanding the processes involved as the plasma so formed evolves in time, is vital for both basic science and a wide variety of applications, including ultrahigh magnetic-field generation, magnetized target fusion, high-current transmission lines, and magnetically accelerated flyer plates. To provide a database for such understanding, Awe *et al.* [1,2] conducted experiments on the University of Nevada, Reno (UNR) Zebra generator (2 TW, 1 MA, 100 ns). The experiments demonstrated plasma initiation and evolution on the surface of thick aluminum wires, i.e., rods, subjected to megagauss magnetic fields. In contrast to the behavior of thin wires currently used in arrays for the production of intense soft x rays [3], a magnetic-field threshold for plasma initiation was observed and determined to be 2.2 MG for nominal magnetic field rise rates that were varied from 30 to 80 MG/ μ s. Furthermore, as the plasma evolved, the surface temperatures observed (e.g., >30 eV) were much higher than the <2 eV that simple analysis suggests for this situation [4]. Although nonthermal processes were eliminated by careful experimental design, the data alone do not provide insight into the underlying physical mechanisms that lead to the initiation of plasma and to the plasma's subsequent behavior. Therefore, in this Letter, we report computational modeling of the UNR Zebra experiments. In contrast to thin wires, where nonthermal mechanisms play an important role, we show that a magnetohydrodynamic (MHD), i.e., "thermal," model can predict plasma initiation at a time consistent with the experimental observations and give insight into the subsequent behavior. Most importantly, we provide the first computational demonstration

of a magnetic-field threshold for plasma initiation on an aluminum surface.

As the MHD equations describing a pulsed magnetic-field experiment are highly coupled and highly nonlinear, reproducing and understanding not only each individual experiment but also the observed trends represents a profound challenge to theory and numerical modeling. Many of the basic challenges in computationally modeling this type of experiment have been elucidated by Garanin *et al.* [5], who computationally demonstrated plasma formation thresholds for copper of 1.6 MG for a constant magnetic-field drive and 3 MG for a drive magnetic field increasing at the rate of 5 MG/ μ s. The computations reported here use a MHD model that simultaneously solves a continuity equation, an equation of motion, Faraday's law, and a material energy equation. Electromagnetic processes are coupled with the Euler equations of hydrodynamics. The equation of motion includes the Lorentz force. A simple Ohm's law is used in Faraday's law: $\vec{E} + \vec{v} \times \vec{B} = \eta \vec{J} = \vec{E}^*$, where \vec{E} is the electric field in the Eulerian frame of reference, \vec{v} is the material velocity, \vec{B} is the magnetic field, η is the resistivity, \vec{J} is the current density, and \vec{E}^* is the electric field in the plasma frame. A separate flux-limited radiation diffusion equation is solved simultaneously with the other equations to determine the total energy radiated from the surface. The model does not include photoionization suggested in [5] to be possibly important but not included in the computations reported there. Although this model does not incorporate any physics that can correctly be called electrical "breakdown," it does lead to solutions that have breakdownlike properties, i.e., a rapid increase in ionization levels.

For closure, the MHD partial differential equations require constitutive relations and transport properties of the material being modeled. Because the equation of state

(EOS), electrical resistivity, thermal conductivity, and opacities of aluminum in the low-density, low-temperature range where plasma forms are not well known, we explore the implications of the best available EOS and transport-coefficient combinations. We use commonly used Los Alamos National Laboratory SESAME format tabular EOSs 3719 and 3799 and Planckian and Rosseland opacities 13716; the EOSs have Maxwell constructs in the vapor dome region. We use two SESAME format versions of the commonly used Lee-More-DesJarlais resistivities and thermal conductivities, version 29371 dated August, 1999 and version 29373, dated July 2001. In addition, we use a new and previously unavailable SESAME format implementation of a version of the resistivity and thermal conductivity models developed at the All-Russian Scientific Research Institute of Experimental Physics (VNIIEF) [5].

All computations reported here are one-dimensional. As discussed in [2], the experimental parameters have been chosen so that one-dimensional behavior is expected and observed until after plasma has formed. The computations have been conducted on a basic MacIntosh laptop computer using a descendant of an Eulerian code that has previously been used to model, among others, the one- and two-dimensional behavior of frozen deuterium wires [6] and the two-dimensional behavior of a Magnetized Target Fusion plasma formation system [7]. The computational method is implicit and does not use fractional time steps. For all computations, 1800 uniform radial cells cover the interior 0.9 mm ($\Delta r = 0.5 \mu\text{m}$). An additional 600 cells cover from 0.9 mm to 1.7 mm. A “cutoff density” of 10^{-3} kg/m^3 is used to define the separation between “real” material and “vacuum.” A 936-kA-peak electrical current characteristic of early Zebra experiments is used for the magnetic-field boundary condition (later experiments reached a higher peak, although the initial rise in current up until the time of plasma formation is similar enough that the computations reported here are valid; the current waveform is independent of the initial rod diameter).

To compare the computed results directly with the experimental results, we use the emission and absorption formulas of Zeldovich and Raizer [8] and the computed profiles to compute the emission in the green-light range and infer an equivalent green-light surface brightness

temperature. Table I summarizes the computations for two EOS/transport-coefficient combinations. For the three rod sizes reported in [2] (0.5, 0.8, 1.0 mm diameter), the 3719/VNIIEF computations (Table I, left) predict very accurately (within 1–2 ns) the time at which the observed brightness temperature reaches 0.75 eV, approximately the value at which, experimentally, the brightness temperature begins a sudden rise indicative of first plasma appearance. The major result of [1] was the demonstration of a threshold magnetic field that must be reached before plasma formation begins. As Table I shows, each EOS/transport combination also computationally demonstrates a magnetic-field threshold for strong plasma formation, although the 3799/29373 combination (Table I, right) shows plasma appearance significantly later than observed. Table I shows that only the magnetic field value is approximately constant when plasma begins to form. The surface electric field varies by more than a factor of 2, and the rate of change of magnetic field at the surface varies by more than an order of magnitude.

Figure 1 compares the temporal profiles of the computational and experimental brightness temperatures. Table I and Fig. 1 show that all EOS/transport combinations show behavior qualitatively similar to the observations. Each combination shows the trend of later plasma beginning and lower peak brightness temperature for increased diameter. Each combination shows an approximate magnetic-field threshold for plasma to begin. Each combination predicts a maximum rod diameter above which no plasma will form; for example, the peak brightness temperature for the 3719/VNIIEF combination is only 3.5 eV at 1.6-mm diameter and 0.17 eV at 2-mm diameter.

For the 0.8-mm-diameter rod [Fig. 1(b)], the computed curve *D* and the experimental curve *E* (a multishot average) are in very good agreement except for a yet unexplained time shift of approximately 6–8 ns (several ns shifts in the data have also been observed in different experimental series). Except for a similar time shift, curves *D* and *E* for 0.5-mm diameter [Fig. 1(a)] and 1.0-mm diameter [Fig. 1(c)] are also in good agreement until the temperature reaches approximately 23 eV [Fig. 1(a)] and 12 eV [Fig. 1(c)]. Because the time at which the computations and the experiment reach 0.75 eV agree much closer

TABLE I. Approximate parameters when plasma first forms for the 3719/VNIIEF combination (left) and the 3799/29373 combination (right). Plasma does not form at 1.6-mm diameter for the 3799/29373 combination.

Rod diam (mm)	Time (ns) when computed green brightness temperature reaches 0.75 eV	Surface magnetic field <i>B</i> (MG)	<i>dB/dt</i> (MG/ μs)	Surface electric field <i>E*</i> (MV/m)
0.5	87.6/95.2	2.47/2.70	51/38	3.4/4.1
0.64	95.2/105.3	2.49/2.68	39/30	3.1/3.3
0.8	103.7/117.4	2.44/2.70	26/26	2.8/3.0
1	114.8/133.6	2.39/2.63	26/23	2.4/2.1
1.25	129.2/161.1	2.36/2.30	15/–7	2.0/1.8
1.6	156.4/–	2.13/–	–3/–	1.3/–

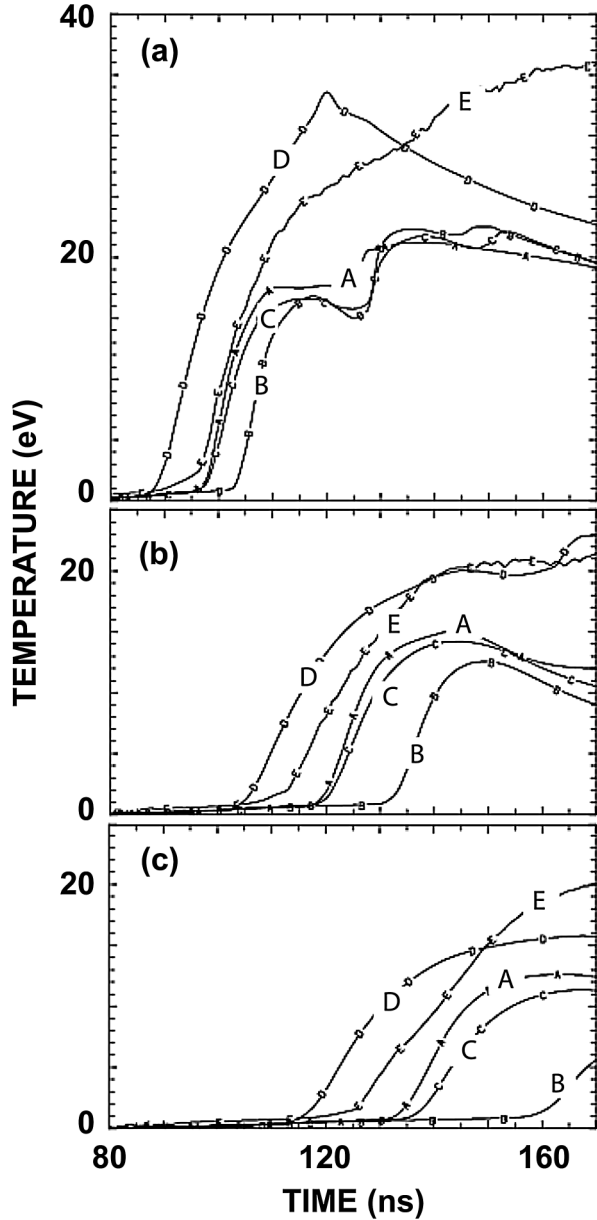


FIG. 1. The green-light brightness temperature, computed using EOS/transport combinations (A) 3719/29371, (B) 3719/29373, (C) 3799/29373, and (D) 3719/VNIIEF for (a) 0.5-mm diameter, (b) 0.8-mm diameter, and (c) 1-mm diameter. The corresponding brightness temperature data from Refs. [1,2] is curve E.

than the overall profile, this time shift apparently results because once plasma formation has begun the experimental temperature rises more slowly than the computational temperature from 0.75 to about 2 eV. Whereas the plasma evolution for the 3719/VNIIEF combination leads the experimental results in time, the evolution for the other combinations trails the experimental results. Because the best available combinations bracket the experimental observations, the major difference between the computations and experiments appears to be uncertainties in the EOSs and transport coefficients. Some of the late-time

disagreement may be due to the higher late-time current in the most recent experiments from which the data were obtained and to instabilities that form in the experiments after plasma has formed.

The plasma formation process in the simulations can be understood by examining characteristic heating and cooling times. The rate of change of the temperature T is given by

$$\frac{dT}{dt} = \left(\frac{\partial T}{\partial \rho}\right)_\varepsilon \frac{d\rho}{dt} + \left(\frac{\partial T}{\partial \varepsilon}\right)_\rho \frac{d\varepsilon}{dt} = T \sum_i \frac{1}{\tau_i},$$

where ρ is the mass density, ε is the specific internal energy, and the τ_i correspond to the various physical processes in the continuity and material energy equations. Prior to and during plasma formation, the dominant processes are given by the Ohmic heating time τ_{Oh} and the expansion cooling time τ_c ,

$$\tau_{\text{Oh}} = \frac{\rho T \eta}{(E^*)^2 (\partial T / \partial \varepsilon)_\rho}; \quad \tau_c = \frac{\rho T}{p \nabla \cdot \bar{v} (\partial T / \partial \varepsilon)_\rho},$$

where p is the material pressure. For a specified value of E^* and $\nabla \cdot \bar{v}$, these characteristic times are functions only of density and temperature, and hence can be plotted in the density-temperature plane similarly to the way EOS and transport quantities are commonly plotted. We can estimate $\nabla \cdot \bar{v}$ as $\alpha v / r$, where α is a multiplier and r is the material radius. From the data reported in [2], we can estimate the expansion velocity at plasma formation as approximately 3 km/s. Values of α and r of 10 and 0.5 mm are reasonable for estimation purposes. $\nabla \cdot \bar{v}$ can readily be scaled to other values of v , α , and r .

Shown in Fig. 2 (top) is τ_{Oh} for the 3719/29371 EOS/transport combination and a 2 MV/m electric field, which is characteristic of the Zebra experiments, as shown in Table I. The τ_{Oh} values for other values of the electric field can be determined by scaling the values in Fig. 2 (top). Under the vapor dome, τ_{Oh} is large. However, Fig. 2 (top) shows that at sufficiently low density when the material is completely vaporized, τ_{Oh} can be subnanosecond. Other EOS/transport combinations have qualitatively similar behavior, although clearly the detailed quantitative differences lead to the differences shown in Fig. 1. As mentioned previously, the time shift in Fig. 1 between the computed results (curve D) and the experimental results (curve E) apparently result because the experimental temperature rises more slowly than the computational temperature from 0.75 to about 2 eV; i.e., the τ_{Oh} in the computations is smaller than in the experiment. This may be an indication that the resistivity in the density-temperature space where τ_{Oh} is subnanosecond may be too low. Hence, the experimental results may help guide the theoretical determination of electrical resistivity in the density-temperature space where theoretical models are not accurate and experimental data are limited.

Figure 2 (bottom) compares the ratio of the expansion cooling time to the Ohmic heating time. For any reasonable values of parameters, the Ohmic heating time is always

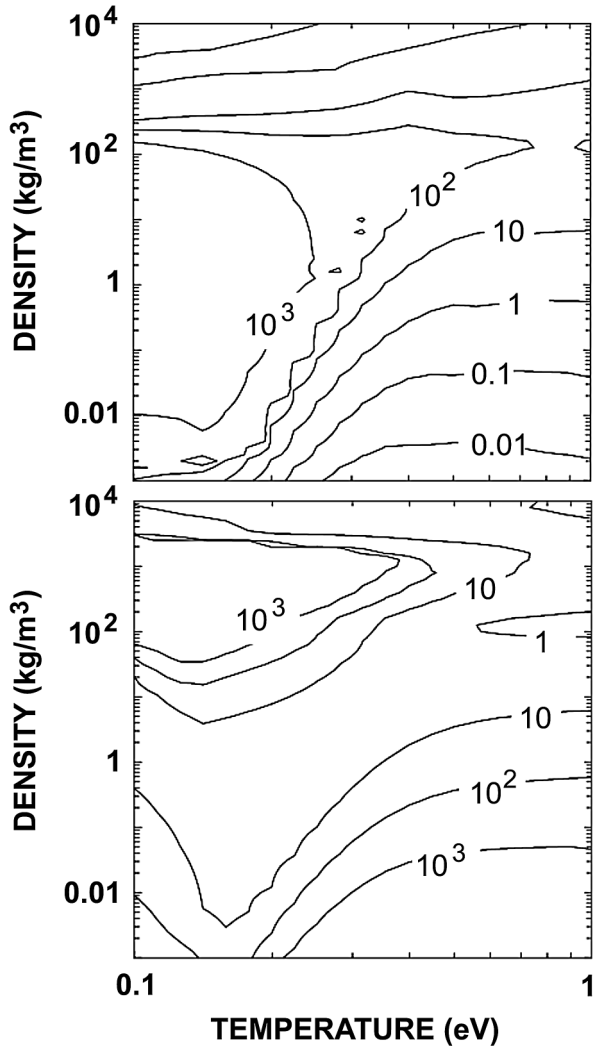


FIG. 2. The characteristic Ohmic heating time τ_{Oh} (ns) for $E^* = 2$ MV/m (top), and the ratio of the characteristic expansion cooling time τ_c to τ_{Oh} for $v = 3$ km/s, $\alpha = 10$, and $r = 0.5$ mm (bottom), based upon the 3719/29371 combination.

smaller than the cooling time; i.e., Ohmic heating exceeds expansion cooling.

The computations and Fig. 2 lead to the following interpretation of the plasma initiation process. Once material has melted, it is resistive enough to expand outward across the magnetic field. An examination of the forces on the outer cells in our simulations shows that the pressure gradient outward force is larger than the inward magnetic force, even though the magnetic pressure $B^2/2\mu_0$ is much larger than the material pressure. On the other hand, as Fig. 2 shows, Ohmic heating, although very low while the material is highly resistive, still exceeds the expansion cooling. Hence net energy is deposited in the material as it expands across the magnetic field; i.e., the expansion process is not adiabatic. If sufficient energy is deposited, the material exits the vapor dome and enters a density-temperature space where the Ohmic heating can rapidly take the low-density material into the plasma state. Lindemuth *et al.* [9] have shown how

the Ohmic heating time decreases at the leading edge of the expanding material as the electric field builds up and as the material slowly heats. Finally, the Ohmic heating time becomes subnanosecond, and plasma forms quickly at the outer edge. The initially optically thin plasma layer grows quickly in width and enclosed mass due to thermal conduction from the initial plasma layer inward, followed by Ohmic heating of the inner material; computations that do not include thermal conduction reach plasma temperatures much higher than 100 eV at the outer edge. The brightness temperature is not determined by the hottest, lowest-density plasma, but by cooler, more dense plasma where the optical depth is comparable to the plasma width, as will be discussed in a future publication. According to the computations, plasma forms before inward-moving shocks and magnetic diffusion waves reach the axis; i.e., plasma forms while the rods are still thick. Prior to disturbances reaching the axis, only a very small fraction of the mass is in the plasma state. We cannot yet offer an explanation of why plasma begins to form at a specific magnetic field value, rather than, for example, a specific value of E^* or dB/dt .

These computations predict satisfactorily experimental observables such as time of plasma initiation, the magnetic-field threshold, and the brightness temperature evolution, and trends in the observables as the rod diameter is varied. With observables and trends so predicted, it seems reasonable to conclude that plasma initiation in the UNR Zebra experiments is a thermal process driven by Ohmic heating and not by other mechanisms, e.g., breakdown of adsorbed hydrocarbons, as often invoked in thin wires; the higher magnetic field combined with the somewhat lower electric field may help prevent nonthermal effects.

We acknowledge informative discussions and/or communications with T. Awe, S. Fuelling, S. Garanin, R. Reinovsky, V. Makhin, M. Frese, S. Kuznetsov, S. Rosenthal, and J. Chittenden. This research was supported by DOE Grants No. DE-FG02-04ER54752, No. DE-FG02-06ER54892, and No. DE-FC52-01NV14050.

- [1] T.J. Awe *et al.*, *Phys. Rev. Lett.* **104**, 035001 (2010).
- [2] T.J. Awe *et al.*, *Phys. Plasmas* **17**, 102507 (2010).
- [3] K. Matzen *et al.*, *Phys. Plasmas* **12**, 055503 (2005).
- [4] H. Knoepfel, *Pulsed High Magnetic Fields* (North-Holland, Amsterdam, 1970).
- [5] S.F. Garanin *et al.*, *J. Appl. Mech. Tech. Phys.* **46**, 153 (2005).
- [6] I.R. Lindemuth, G.H. McCall, and R.A. Nebel, *Phys. Rev. Lett.* **62**, 264 (1989); I.R. Lindemuth, *Phys. Rev. Lett.* **65**, 179 (1990).
- [7] I.R. Lindemuth *et al.*, *Phys. Rev. Lett.* **75**, 1953 (1995).
- [8] Ya.B. Zeldovich and Yu.P. Raizer, *Physics of Shock Waves and High-Temperature Hydrodynamic Phenomena* (Dover, Mineola, NY, 2002).
- [9] I.R. Lindemuth *et al.*, in *17th IEEE Power Conference*, Technical Digest (IEEE, New York, 2009), No. O8-1, p. 193.